An Investigation of Lateral Geniculate Nucleus Volume in Patients With Primary Open-Angle Glaucoma Using 7 Tesla Magnetic Resonance Imaging

Jong Yeon Lee,[1] Hye Jin Jeong,[2] Jong Hwan Lee,[1] Yu Jeong Kim,[1] Eung Yeop Kim,[3] Yong Yeon Kim,[4] Taekhyun Ryu,[2] Zang-Hee Cho,[2] and Young-Bo Kim[2]

[1]Department of Ophthalmology, Gachon University, Gil Hospital, Incheon, Korea
[2]Neuroscience Research Institute, Gachon University, Incheon, Korea
[3]Department of Radiology, Gachon University, Incheon, Korea
[4]Department of Ophthalmology, Korea University College of Medicine, Seoul, Korea

Correspondence: Young-Bo Kim, Neuroscience Research Institute, Gachon University, #1198, Kuwol-dong, Namdong-ku, Incheon, 405-760, Korea; neurokim@gachon.ac.kr.

Submitted: January 7, 2014
Accepted: April 3, 2014

Citation: Lee JY, Jeong HJ, Lee JH, et al. An investigation of lateral geniculate nucleus volume in patients with primary open-angle glaucoma using 7 tesla magnetic resonance imaging. *Invest Ophthalmol Vis Sci*. 2014;55:3468–3476. DOI: 10.1167/iovs.14-13902

Purpose. To investigate lateral geniculate nucleus (LGN) volume of primary open-angle glaucoma (POAG) patients compared with age- and sex-matched controls using ultra-high field 7.0-T magnetic resonance imaging (MRI).

Methods. The study included 18 patients with POAG and 18 age- and sex-matched healthy volunteers. All subjects underwent imaging on a high-resolution 7.0-T MRI system. Bilateral LGNs were identified and manually delineated, and LGN volumes were compared. Peripapillary retinal nerve fiber layer (pRNFL) thickness, optic nerve head parameters (including optic disc size, rim area, and cup-to-disc ratio), and combined thickness of the ganglion cell layer and inner plexus layer (GC-IPL) were measured by Cirrus high-definition optical coherence tomography (OCT). Correlations between OCT parameters and LGN volume were investigated.

Results. Mean LGN volumes were significantly smaller in the POAG group than in the control group (right, glaucoma 83.97 mm^3 [SD $\pm$ 26.65] versus control 106.12 mm^3 [SD $\pm$ 24.32]; left, glaucoma 65.12 mm^3 [SD $\pm$ 29.41] versus control 92.70 mm^3 [SD $\pm$ 24.42], both $P < 0.05$). In the POAG group, average GC–IPL thickness was correlated with contralateral LGN volume (right LGN: $r = 0.605$, $P = 0.008$; left LGN: $r = 0.471$, $P = 0.049$). The correlation for right LGN volume remained significant after correction for multiple comparisons. However, there was no correlation between LGN volume and average pRNFL thickness or optic disc parameters in the POAG group.

Conclusions. On high-resolution 7.0-T MRI, LGN volumes in POAG patients are significantly smaller than those of healthy subjects. Furthermore, in patients, LGN volume was found to be significantly correlated with GC–IPL thickness of the contralateral eye.

Keywords: glaucoma, lateral geniculate nucleus, retinal nerve fiber layer thickness, ganglion cell layer, inner plexiform layer, GC-IPL, optical coherence tomography, 7 tesla magnetic resonance imaging

Retinal ganglion cell (RGC) degeneration is the major pathogenetic characteristic of glaucoma.[1–18] Most RGCs synapse the next neurons in the lateral geniculate nucleus (LGN), which serves as an important relay station to visual cortex.[19] Previous studies have reported decreased neuronal size and numbers in LGN and overall LGN shrinkage in an experimental glaucoma monkey model.[20–23] Postmortem pathologic studies for human glaucoma have also reported decreased LGN volumes and neuronal cell densities in LGN.[24,25]

Since Horton et al.[26] first detected the LGN in vivo using MRI with proton density (PD)-weighted images, several studies have attempted to describe the LGN in detail.[26–33] The LGN is a small, deep subcortical structure that contains myelinated fibers surrounded by white matter tracts including the optic tract, optic radiation, and the posterior limb of internal capsule, which makes it difficult to identify the LGN on magnetic resonance (MR) images.[27] In addition, since the LGN height is 4 to 6 mm, measuring LGN height would have a potential bias, especially with low resolution on MR images; we thought that the ultra-high field PD-weighted MRI could allow us to investigate the volume of LGN with higher accuracy. To our knowledge, there has been no study to investigate LGN degeneration in glaucoma patients with ultra-high field MRI.

Gupta et al.[34] reported the first in vivo MRI evidence of the LGN degeneration with reduced height in glaucoma patients. Several researchers have demonstrated relationships between LGN volume/height in vivo and structural or functional parameters of glaucomatous changes.[35–39] Recent advances in OCT technology have enabled quantitative assessment of the macular ganglion cell–inner plexiform layer (GC-IPL) thickness as well as RNFL thickness and optic nerve head parameters. It is well known that the pathogenesis of glaucoma involves the degeneration of cell bodies, dendrites, and axons

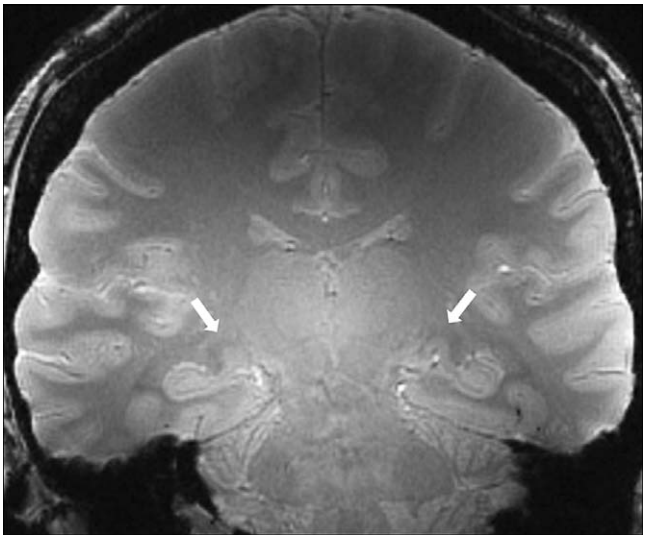

FIGURE 1. A representative coronal proton density–weighted image showing the bilateral lateral geniculate nuclei (*arrows*) in a healthy subject at 7.0 Tesla MRI.

located in the ganglion cell layer, inner plexiform layer, and RNFL, respectively. However, investigations on the nature of the association between in vivo LGN degeneration and structural changes of retinal layers and optic nerve head in glaucoma are still limited.

Thus, we aimed to investigate the difference of LGN volume between primary open-angle glaucoma (POAG) patients and healthy controls using 7.0-T MR imaging and also to investigate the relationship between the LGN volume and the structural parameters of glaucomatous changes, including peripapillary retinal nerve fiber layer (pRNFL) thickness, optic disc parameters, and ganglion cell–inner plexiform layer (GC-IPL) thickness determined by spectral-domain optical coherence tomography (SD-OCT) in POAG.

SUBJECTS AND METHODS

This prospective study was conducted at the Department of Ophthalmology and Neuroscience Research Institute at Gachon University. The legal and ethical aspects of the study were reviewed and approved by the Institutional Review Board (IRB) of Gachon University and by the Korean Food and Drug Administration (KFDA). This study adhered to the tenets of the Declaration of Helsinki. Patients with POAG and an age- and sex-matched control group were recruited from the Department of Ophthalmology at Gil Hospital, Gachon University. Subjects were interviewed to determine medical and psychological histories including body weights and heights. The exclusion criteria included age of <20 years; a history of any neurologic disorder including stroke and Alzheimer's disease; a history of claustrophobia or other psychological disorder; and having metallic material in the body including a pacemaker, a dental implant, or an artificial heart valve. Informed consent was provided by all study subjects prior to study commencement.

Glaucoma Group

All patients underwent comprehensive ophthalmic examinations of both eyes, including best-corrected visual acuity, refractive error, slit-lamp biomicroscopy, central cornea thickness with a noncontact specular microscope (SP-3000P; Topcon, Tokyo, Japan), gonioscopy, Goldmann applanation tonometry, Humphrey Swedish interactive threshold algorithm (SITA) 30-2 testing (Zeiss-Humphrey, San Leandro, CA, USA), dilated red-free photography, stereoscopic optic disc photography, SD-OCT scanning (Cirrus HD-OCT; Carl Zeiss Meditec, Inc., Dublin, CA, USA), and axial length with partial coherence interferometry (IOL Master; Carl Zeiss Meditec AG, Jena, Germany). Glaucoma was diagnosed when glaucoma hemifield test results were outside the normal limits or the standard deviation had a *P* value less than 0.05; or when there was a cluster of three points or more in the pattern of the deviation plot in a single hemifield with a *P* value less than 0.05, one of which had to have a *P* value less than 0.01 on the Humphrey

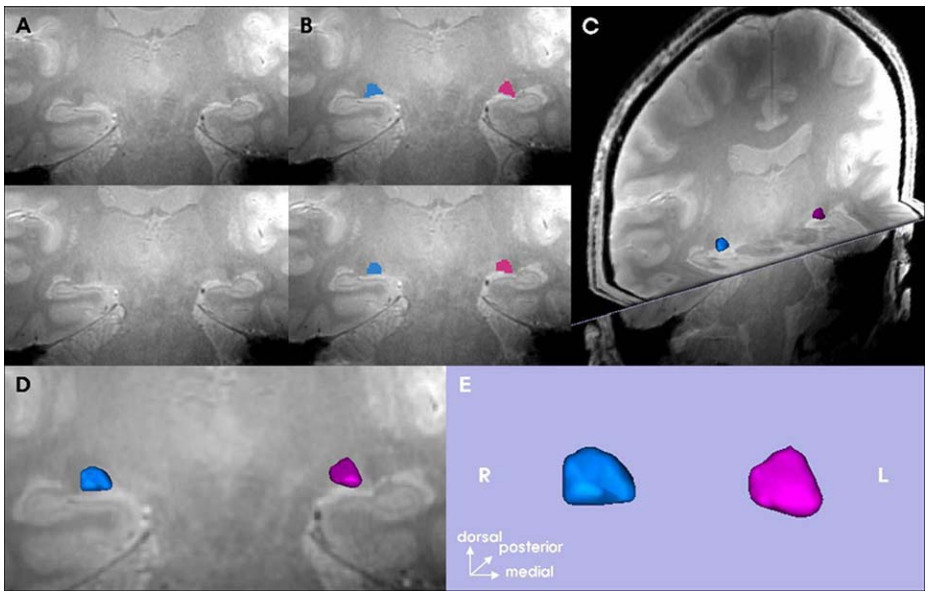

FIGURE 2. A mimetic diagram for measuring volume of the lateral geniculate nucleus. (**A**) Coronal proton density–weighted images showing the LGN in both sides. (**B**) Manual segmentation of the LGN in selected slices. (**C–E**) LGN segmentation by 3-D slicer.

Investigative Ophthalmology & Visual Science

Table 1. Baseline Characteristics

	POAG, $n = 18$	Control, $n = 18$	*P*
Age, y	47.6 ± 13.3	45.2 ± 10.9	0.673*
Sex, male/female	8/10	8/10	1.000†
Body weight, kg	65.1 ± 14.7	62.0 ± 11.8	0.584*
Body height, cm	163.7 ± 10.1	162.8 ± 9.3	0.888*
Visual acuity, logMAR			
Right eye	0.02 ± 0.06	0.01 ± 0.02	0.563*
Left eye	0.10 ± 0.35	0.01 ± 0.02	0.563*
Refractive error, diopters			
Right eye	−2.37 ± 3.06	−1.69 ± 2.20	0.650*
Left eye	−1.78 ± 2.51	−1.65 ± 2.06	0.963*
Axial length, mm			
Right eye	24.30 ± 1.54	24.07 ± 0.94	0.657*
Left eye	24.30 ± 1.54	24.05 ± 0.91	0.631*

Data are presented as means ± standard deviation. Refractive error, spherical equivalent.

* Mann-Whitney *U* test.

† χ^2 test.

SITA 30-2 test[40]; and/or a nerve fiber layer defect combined with a corresponding optic disc change.

One macular scan and one optic disc scan were performed using a Cirrus HD-OCT instrument (software version 6.0; Carl Zeiss Meditec, Inc.). For ganglion cell analysis, three-dimensional (3-D) macular cube OCT data were obtained using the macular cube 512 × 128 scan mode. The GC–IPL algorithm automatically indentifies the outer boundary of the RNFL and the outer boundary of the IPL. The GC–IPL thickness is calculated as the distance between the two boundaries. The segmentation procedure operates in three dimensions and uses a graph-based algorithm to identify each layer. The average, minimum (lowest GC–IPL thickness over a single meridian crossing the annulus), and sectoral (superotemporal, superior, superonasal, inferonasal, inferior, inferotemporal) thicknesses are measured in an elliptic annulus (dimensions, vertical inner and outer radius of 0.5 and 2.0 mm, horizontal inner and outer radius of 0.6 and 2.4 mm, respectively). The size and shape of the elliptical annulus were chosen to conform closely to the histologic macular anatomy, and the annulus corresponds to the area where the RGC layer is thickest in normal eyes.[41–43] The pRNFL thickness was measured in optic disc cube 200 × 200 scan mode, which consisted of 40,000 axial scans (in a 6 × 6 × 2 mm cube) centered on the optic disc. Average, quadrants, and clock-hour sector RNFL thicknesses on a measurement circle 3.46 mm in diameter are calculated. Optic nerve head parameters were measured using the same scanning protocol (using the same 6 × 6 data cube) as used for RNFL analysis. Cirrus HD-OCT automatically indentifies the termination of Bruch's membrane and considers this to be the optic disc edge. The Cirrus HD-OCT algorithm measures optic disc rim area by measuring the rim width within the circumference the optic disc edge. Average cup-to-disc ratio (CDR) and optic disc cup volume are also automatically determined using this algorithm. Subjects who met any of following criteria were excluded: any retinal disease, any history of neurologic disease, macular edema or another vitreoretinal disease, OCT images with low signal strength of <6, lost data on the peripapillary ring, obvious motion artifact or incorrect segmentation. The mean age of glaucoma patients was 47.6 ± 13.3 years (8 men and 10 women).

Table 2. Comparison of Lateral Geniculate Nucleus Volume, Average and Quadrant RNFL Thicknesses, and Optic Nerve Head Parameters Measured by Cirrus HD-OCT for POAG Patients and Normal Healthy Controls

	POAG, $n = 18$	Control, $n = 18$	*P**
LGN vol R, mm^3	83.97 ± 26.65	106.12 ± 24.32	0.029
LGN vol L, mm^3	65.12 ± 29.41	92.70 ± 24.42	0.008
pRNFL thickness, μm			
Average R	75.56 ± 16.93	97.17 ± 6.85	<0.001
Average L	70.44 ± 13.44	96.78 ± 7.85	<0.001
Superior R	90.28 ± 27.28	117.17 ± 13.26	0.001
Temporal R	64.11 ± 14.27	73.44 ± 12.24	0.020
Inferior R	85.06 ± 27.87	129.56 ± 12.01	<0.001
Nasal R	64.61 ± 10.87	69.17 ± 11.00	0.203
Superior L	78.83 ± 23.30	122.22 ± 16.04	<0.001
Temporal L	57.78 ± 10.50	70.17 ± 17.64	0.003
Inferior L	83.61 ± 23.88	128.61 ± 11.09	<0.001
Nasal L	60.44 ± 8.56	68.56 ± 11.96	0.040
ONH parameters			
Disc area R, mm^3	2.04 ± 0.65	1.82 ± 0.41	0.265
Disc area L, mm^3	2.15 ± 0.66	1.81 ± 0.39	0.059
Rim area R, mm^3	0.80 ± 0.33	1.29 ± 0.28	<0.001
Rim area L, mm^3	0.85 ± 0.29	1.31 ± 0.31	<0.001
Average CDR, R	0.75 ± 0.12	0.47 ± 0.21	<0.001
Average CDR, L	0.74 ± 0.18	0.46 ± 0.22	<0.001

Data are presented as mean ± standard deviation. Vol, volume; ONH, optic nerve head.

* Mann-Whitney *U* test.

Control Group

All healthy volunteers underwent ophthalmological examinations including visual acuity, refractive error, slit-lamp biomicroscopy with Goldmann applanation tonometry, fundus examination, axial length, pRNFL thickness, optic disc parameters, and macular ganglion cell–inner plexiform layer (GC-IPL) thickness with Cirrus HD-OCT to rule out glaucoma and any other ocular diseases except cataract. Two of the potential controls with finding suspicious for glaucoma on these examinations were excluded. Eighteen healthy, nonglaucomatous, age- and sex-matched volunteers were recruited as study controls. Mean age of the control group was 45.2 ± 10.9 years (8 men and 10 women).

MRI Acquisition

A 7 Tesla research prototype MRI scanner (Magnetom 7T; Siemens, Erlangen, Germany) was used with an optimized eight-channel radiofrequency coil designed specifically for this study. The specific MR imaging parameters used were as follows: coronal PD-weighted imaging (TR/TE = 35.3 / 3.75 ms; flip angle = 6°; slice thickness = 0.6 mm without gap; 320 × 320 matrix; total acquisition time 4 minutes, 4 seconds). The LGN was identified according to the published landmarks (Fig. 1)[26,44,45]: It was located above the hippocampus and the ambient cistern, beneath and lateral to the thalamus, and medial to the optic radiations. All subjects' MRI data were submitted to a neurologist (YK) to rule other pathologies that are known to present as glaucoma. An experimenter (HJJ) blinded to the information on subjects measured the volume of LGN using a 3-D slicer (http://www.slicer.org [in the public domain]). On each scan section on which the LGN was visible, its area was manually segmented using 3-D slicer as shown in

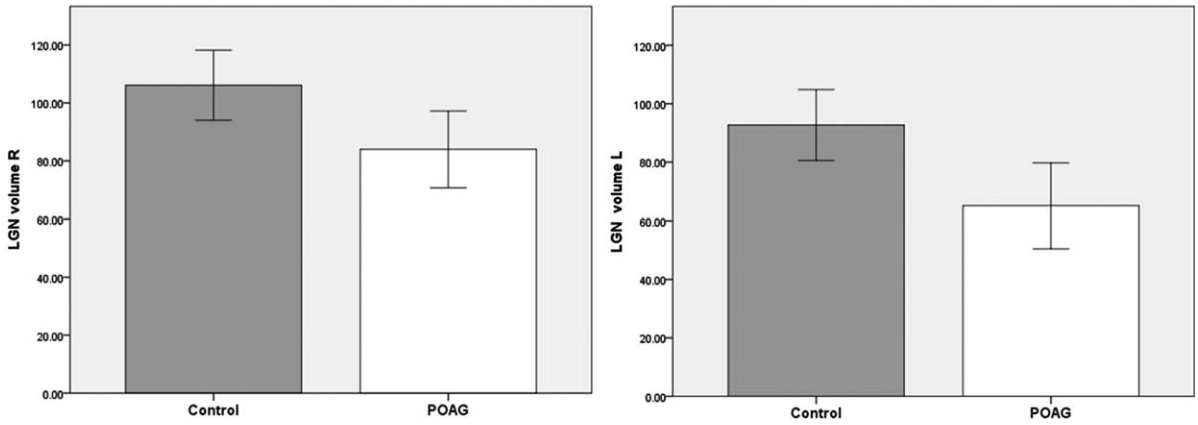

Figure 3. Bar graphs of right and left LGN volumes in POAG and control groups. Each bar represents mean volume of LGN in control and POAG group, and error bar indicates 95% confidence interval.

Figure 2. Data were processed using MATLAB (version 7.8.0.347; The MathWorks, Natick, MA, USA).

Statistical Analysis

Group baseline characteristics such as mean age, sex, ocular parameters, and LGN volumes were compared using the Mann-Whitney *U* test for continuous variables and Pearson χ^2 tests for categorical data. The normality of distribution of the variables was assessed by a Kolmogorov-Smirnov test. Statistical correlation between LGN volumes versus the structural changes of glaucoma determined by Cirrus HD-OCT was obtained via a Pearson correlation test. Multiple correlations were investigated between LGN volume versus average GC-IPL, average RNFL thickness, and average CDR. The *P* value was adjusted using the false discovery rate approach described by Benjamini and Hochberg.[46] For subanalyses of associations between topographical parameters and LGN volume, the RNFL parameters included in the analysis were average and quadrant thicknesses; and the GC–IPL parameters considered were average, minimum, and sector perimacular thicknesses. In addition, the optic nerve head parameters were disc area, rim area, and average CDR. For each analysis, the *P* value was also adjusted using the false discovery rate. The LGN volumes of 16 subjects were measured by another grader. The intraclass correlation coefficients (ICC) for LGN volume were calculated to assess agreements between the two graders. All statistical analyses were performed using SPSS version 17.0 (SPSS, Inc., Chicago, IL, USA). A *P* value less than 0.05 was considered statistically significant.

Results

The baseline characteristics of the 36 study subjects are summarized in Table 1. Age, sex, body weight, body height, visual acuity, refractive error, and axial length did not differ between the POAG and control groups. Mean volumes of both right and left LGNs in patients were significantly smaller than those in controls (Table 2, Fig. 3). Average pRNFL thickness on both eyes of the POAG group were significantly thinner than those of controls (both $P < 0.001$). Quadrant pRNFL thicknesses were also significantly thinner in POAG than those in controls except for nasal quadrant of the right eye. There was no difference in disc area between the two groups. Rim areas and CDR in the POAG group were significantly smaller than in the control group (both $P < 0.001$). Table 3 lists average, minimum, and sector GC–IPL thicknesses. Average, minimal, and all sector GC–IPL thicknesses in the POAG group were significantly thinner than in the control group.

In the POAG group, LGN volume was significantly correlated with average GC–IPL thickness of the contralateral eye (Table 4). The correlation for right LGN volume remained significant after controlling the false discovery rate for multiple comparison. Figure 4 shows scatter plots of associations between LGN volume versus average GC–IPL thickness, average RNFL thickness, and average CDR in the POAG group. In sector analysis, superior sector GC–IPL thicknesses in left eyes were most correlated with right LGN volume, whereas inferonasal sector GC–IPL thicknesses in right eyes were most correlated with left LGN volume (Table 5). After adjusting with the false discovery rate, superior sector, average, and minimal GC–IPL thicknesses of the left eye were significantly correlated with LGN volume.

There was no correlation between the LGN volume and average pRNFL thickness (Table 6). Superior quadrant RNFL thickness in the left eye was correlated only with right LGN volume. However, the correlation was not significant after correction for multiple comparisons.

Table 3. Comparison of GC-IPL Thicknesses Between POAG Patients and Normal Healthy Controls Measured by Cirrus HD-OCT

GC-IPL Thickness	POAG, $n = 18$	Control, $n = 18$	P^*
Average R	68.22 ± 14.40	81.61 ± 4.90	<0.001
Average L	67.78 ± 11.42	82.11 ± 4.10	<0.001
Minimal R	60.78 ± 20.42	79.00 ± 5.25	<0.001
Minimal L	60.78 ± 13.44	80.56 ± 5.15	<0.001
Superotemporal R	66.61 ± 14.45	80.83 ± 4.81	0.001
Inferotemporal R	65.44 ± 15.15	82.33 ± 6.08	<0.001
Inferior R	65.78 ± 14.71	79.78 ± 4.48	<0.001
Inferonasal R	68.22 ± 18.37	82.17 ± 4.91	0.001
Superonasal R	72.89 ± 14.48	83.50 ± 5.42	0.006
Superior R	69.94 ± 13.77	81.89 ± 6.06	0.001
Superonasal L	71.94 ± 13.13	84.56 ± 4.18	0.005
Inferonasal L	68.89 ± 12.27	82.89 ± 4.40	<0.001
Inferior L	65.44 ± 11.06	80.33 ± 4.84	<0.001
Inferotemporal L	64.61 ± 12.69	82.33 ± 5.15	<0.001
Superotemporal L	66.61 ± 13.66	81.00 ± 4.85	0.001
Superior L	69.61 ± 12.99	82.83 ± 3.96	0.002

Data are presented as mean ± standard deviation.
* Mann-Whitney *U* test.

Table 4. Correlations Between Lateral Geniculate Nucleus Volumes Versus Average GC-IPL Thickness, Average pRNFL Thickness, and Average CDR Measured by Cirrus HD-OCT in POAG

	LGN Volume R			LGN Volume L		
	R	***P* Value**	**Pa**	***R***	***P* Value**	**Pa**
Average GC-IPLT R	0.435	0.071	0.174	0.471	0.049	0.294
Average GC-IPLT L	0.605	0.008	0.048	0.240	0.338	0.676
Average pRNFLT R	0.282	0.256	0.384	0.374	0.126	0.378
Average pRNFLT L	0.415	0.087	0.174	0.104	0.682	0.768
Average CDR R	−0.232	0.354	0.425	−0.102	0.686	0.768
Average CDR L	−0.164	0.515	0.515	0.075	0.768	0.768

Adjusted P value < 0.05 was significant. Pearson's correlation test. GC-IPLT, ganglion cell and inner plexiform layer thickness; pRNFLT, peripapillary retinal nerve fiber layer thickness. Pa, adjusted P value after controlling the false discovery rate for multiple comparisons (six correlations).

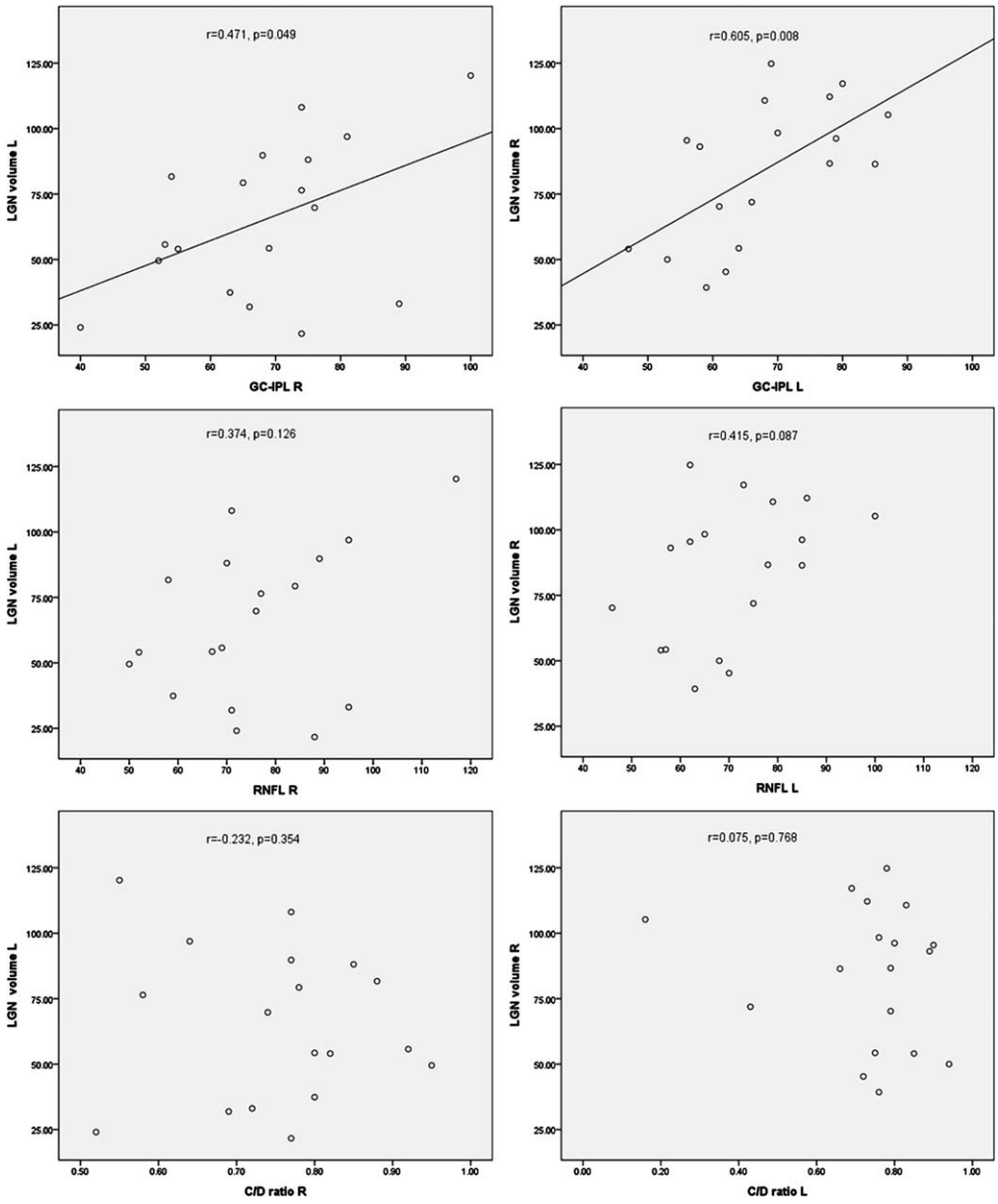

Figure 4. Scatter plots to illustrate correlations between LGN volume versus average GC-IPL, average RNFL thickness, and average cup-to-disc ratio (CDR) in POAG. Correlation coefficients (r) and P values are shown.

Table 5. Correlations Between Lateral Geniculate Nucleus Volumes Versus Average, Minimal, and Sector GC-IPL Thicknesses Measured by Cirrus HD-OCT in POAG

	LGN Volume R			LGN Volume L		
GC-IPL Thickness	***R***	***P***	**Pa**	***R***	***P***	**Pa**
Average R	0.435	0.071	0.094	0.471	0.049	0.182
Average L	0.605	0.008	0.040	0.240	0.338	0.416
Minimal R	0.421	0.082	0.094	0.482	0.043	0.182
Minimal L	0.635	0.005	0.040	0.340	0.167	0.252
Superotemporal R	0.434	0.072	0.094	0.411	0.091	0.194
Inferotemporal R	0.505	0.032	0.073	0.456	0.057	0.182
Inferior R	0.460	0.055	0.094	0.479	0.044	0.182
Inferonasal R	0.318	0.198	0.198	0.483	0.042	0.182
Superonasal R	0.325	0.189	0.198	0.410	0.091	0.194
Superior R	0.436	0.071	0.198	0.404	0.097	0.194
Superonasal L	0.489	0.039	0.198	0.098	0.699	0.746
Inferonasal L	0.426	0.078	0.198	0.047	0.853	0.853
Inferior L	0.512	0.030	0.198	0.336	0.173	0.252
Inferotemporal L	0.589	0.010	0.130	0.353	0.150	0.252
Superotemoral L	0.573	0.013	0.156	0.188	0.455	0.520
Superior L	0.670	0.002	0.032	0.266	0.285	0.380

Adjusted P value < 0.05 was significant. Pearson's correlation test. Pa, adjusted P value with controlling the false discovery rate for multiple comparisons (16 correlations).

No correlation was found between LGN volume and optic nerve head parameters by Cirrus HD-OCT including disc area, rim area, and average CDR before and after correction for multiple comparisons (Table 7). For the 32 LGNs of 16 subjects, ICC for LGN volume was high (ICC for right and left LGNs were 0.889 and 0.898, respectively; both $P < 0.001$).

Discussion

High-resolution MRI shows that POAG patients exhibit a significant reduction in LGN volume compared to age- and sex-matched healthy controls, and that in POAG patients, LGN volume is significantly correlated with macular GC–IPL thickness in contralateral eyes. These results confirm the notion that transsynaptic degenerative change of LGN is involved in the pathophysiology of glaucoma, which is in line with the findings of previous studies.[20–25,34–39] Experimental studies in primates have demonstrated LGN atrophy in glaucoma.[20–23] Gupta et al.[25,34] reported this finding in humans by both postmortem histopathologic study and in vivo MRI study. Several researchers have reported similar results and investigated the relationships between degenerative LGN changes and the functional and structural changes of human glaucoma with various methodologies. Dai et al.[35] found that the LGN height/volume was correlated with functional glaucoma stage, whereas Hernowo et al.[37] showed no significant correlation between visual field sensitivity and LGN volume. Chen et al.[39] reported that both right and left LGN heights were significantly correlated with CDR and RNFL thickness. However, LGN volume was correlated with CDR and RNFL thickness only in left eyes.

The present study showed that LGN volume was correlated with GC–IPL thickness rather than pRNFL thickness. The pathogenesis of glaucoma involves the degeneration of cell bodies and dendrites located within the ganglion cell and inner plexiform layers. This finding suggests that the depletion of RGCs and their dendrites might be synchronized with the depletion of LGN neurons rather than peripapillary RNFL thickness. There are possible explanations. First, the RNFL thickness measured by OCT includes nonneuronal supporting tissues and large blood vessels, as well as RGC axons. In contrast, the macula has relatively small blood vessels and a large number of ganglion cells. These anatomic differences

Table 6. Correlations Between Lateral Geniculate Nucleus Volumes Versus Average and Quadrant pRNFL Thicknesses Measured by Cirrus HD-OCT in POAG

	LGN Volume R			LGN Volume L		
pRNFL Thickness	***R***	***P***	**Pa**	***R***	***P***	**Pa**
Average R	0.282	0.256	0.427	0.374	0.126	0.627
Average L	0.415	0.087	0.420	0.104	0.682	0.729
Superior R	0.314	0.205	0.427	0.409	0.092	0.627
Temporal R	−0.079	0.754	0.754	0.152	0.548	0.729
Inferior R	0.302	0.223	0.427	0.325	0.188	0.627
Nasal R	0.130	0.608	0.754	0.088	0.729	0.729
Superior L	0.531	0.023	0.230	0.219	0.390	0.729
Nasal L	0.254	0.310	0.443	0.132	0.601	0.729
Inferior L	0.375	0.126	0.420	0.135	0.592	0.729
Temporal L	0.088	0.728	0.754	−0.132	0.602	0.729

Adjusted P value < 0.05 was significant. Pearson's correlation test. Pa = adjusted P value with controlling the false discovery rate for multiple comparisons (10 correlations).

Investigative Ophthalmology & Visual Science

Table 7. Correlations Between Lateral Geniculate Nucleus Volumes Versus Average CDR and Disc and Rim Areas Measured by Cirrus HD-OCT in POAG

	LGN Volume R			LGN Volume L		
ONH Parameters	***R***	***P***	**Pa**	***R***	***P***	**Pa**
Average CDR R	−0.232	0.354	0.773	−0.102	0.686	0.922
Average CDR L	−0.164	0.515	0.773	0.075	0.768	0.922
Disc area R	0.047	0.852	0.852	0.098	0.699	0.922
Disc area L	0.059	0.816	0.852	0.081	0.750	0.922
Rim area R	0.287	0.248	0.773	0.260	0.298	0.922
Rim area L	0.172	0.496	0.773	−0.015	0.952	0.952

Adjusted P value < 0.05 was significant. Pearson's correlation test. Pa, adjusted P value with controlling the false discovery rate for multiple comparison (6 correlations).

could be related to our finding. Second, this finding may be line with the greater representation of the central retina in the LGN.[47,48] Kupfer[49] reported that the region of the LGN representing the macula accounts for the posterior two-thirds to three-fourths of the volume of the LGN. Hickey and Guillery[50] reported that the central 15° occupied one-half of the volume, and Schneider et al.[51] reported that the central 15° of visual field occupied 79.5% of the total volume of LGN. Thus, volumetric changes of the LGN may be related more to central retina changes than to peripheral retina changes. The present study also showed that LGN volume was correlated with contralateral GC–IPL thickness rather than ipsilateral thickness. It may be related to topographic distributions of RGCs, whose density is higher in nasal retina than in temporal retinas based on the fovea.[43]

Chen et al.[39] reported that LGN height was significantly correlated with RNFL thickness, as obtained by Stratus OCT and CDRs measured on fundus photography. In that study, LGN volume was found to be correlated with CDR and RNFL thickness only for the left eyes. The discrepancy between these authors' findings and ours could be due to methodological and subject differences. Different resolution used in imaging LGN could render different numbers of sections of LGN visible. Alternatively, the small sample size with a relatively narrow range of RNFL thickness in our study could be a cause of lack of significant correlation between LGN volume and average RNFL thickness or optic disc parameters. Use of a behavioral measure with Humphrey visual field testing as a diagnostic criterion was likely to affect subject selection. In addition, intereye asymmetries of glaucomatous damage and various locations of glaucomatous damage in the retina and optic nerve head among patients might also have influenced outcomes. In the previous study, it was suggested that LGN height measurement might be straightforward and more clinically useful because it is easier to measure height than volume. We agree with this suggestion, but we consider measurement of volume to better represent the general status of the LGN, although it is more time-consuming.

The mean LGN volume of healthy controls in the present study is comparable to volumes reported in postmortem studies. Putnam[52] reported a volume range of 77 to 115 mm^3 in three subjects; Zvorykin[53] reported one of 66 to 152 mm^3 in 17 subjects; and Andrews et al.[54] reported means of right and left LGN volumes of 121 mm^3 (91.1–154 mm^3) and 115 mm^3 (91.9–157 mm^3), respectively. However, our estimates are smaller than those provided by previous in vivo MRI studies. Hernowo et al.[37] reported an average volume of 149 mm^3 using 3T MRI with automated segmentation and voxel-based morphometry. Dai et al.[35] segmented LGNs manually, as in the present study, and reported a volume of 143 mm^3 by 3T MRI with a PD sequence. Zhang et al.[38] reported a mean volume of 154.2 mm^3 for 28 individuals by 1.5T MRI with manual segmentation. Naturally, subject differences such as age differences could have influenced the estimates because a 2- to 3-fold variation in the volume of LGN has been reported among individuals.[53,54] On the other hand, the differences between the present study and previous in vivo neuroimaging studies could be explained by voxel size. We measured LGNs using 0.6-mm isotropic voxels, whereas 1.0-mm or greater slice thicknesses were used in previous studies. This larger slice thickness leads to partial volume effects that make the LGN larger, because it might not allow measurement of its smallest aspects.

In the present study, left LGN volumes were significantly smaller than right LGN volumes in healthy controls. This is consistent with a previous report issued by Li et al.,[55] although the methodologies used differed. In the present study, mean minimum GC–IPL thickness of right eyes was significantly thinner than that of left ones, albeit it was quite a small difference of 1.56 μm, in healthy controls ($P = 0.015$). We could not find any differences for other parameters examined in both eyes. Further larger-scale studies are required to determine the relationship between GC–IPL thickness and LGN volume.

This study has a number of limitations. First, the sample size was relatively small. It was hard to enroll subjects because the ultra high magnetic field MRI could not be performed in subjects with any metallic materials such as a dental implant. Nevertheless, a significant difference in LGN volume was found between groups. However, our sample may not have been large enough to allow detection of a correlation between LGN volumes and both RNFL thickness and optic disc parameters. Thus, larger-scale studies could yield different observations. Second, manual delineation is subject to potential bias. We could not completely exclude the possibility of an erroneous measurement during manual delineation even on 7 Tesla MR imaging. However, it is generally accepted that manual delineation of LGN provides accurate results. Furthermore, interobserver agreement for LGN volume was high in the present study. Thus, such bias was not likely to influence our data substantially. Third, the clinical implications of LGN changes in glaucoma still need to be investigated. However, since LGN would play a role in perception and cognition, including visual attention and awareness, beyond that of a relay nucleus,[56] we suppose that the macular GC–IPL thickness-related LGN changes could be related to perception and cognition of glaucoma patients. Further studies are required to explore implications of the visual pathway involvement beyond the optic nerve in glaucoma patients.

In conclusion, we have shown that LGN volume significantly decreased in POAG compared with normal healthy controls, and that macular GC–IPL thickness was correlated with contralateral LGN volume in POAG using 7T MR imaging. Our findings support the idea that transsynaptic degeneration

is involved in the pathogenesis of POAG and suggest that LGN volumetric changes could depend on macular GC–IPL thickness rather than peripapillary RNFL thickness. Further studies are required to explore implications of the relationship to perception and cognition of glaucoma patients.

Acknowledgments

Supported by Gachon University Gil Medical Center Research Grant 2013-13.

Disclosure: **J.Y. Lee**, None; **H.J. Jeong**, None; **J.H. Lee**, None; **Y.J. Kim**, None; **E.Y. Kim**, None; **Y.Y. Kim**, None; **T. Ryu**, None; **Z.-H. Cho**, None; **Y.-B. Kim**, None

References

1. Quigley HA, Dunkelberger GR, Green WR. Retinal ganglion cell atrophy correlated with automated perimetry in human eyes with glaucoma. *Am J Ophthalmol*. 1989;107:453–464.
2. Dandora L, Hendrickson A, Quigley HA. Selective effects of experimental glaucoma on axonal transport by retinal ganglion cells to the dorsal lateral geniculate nucleus. *Invest Ophthalmol Vis Sci*. 1991;32:1593–1599.
3. Glovinsky Y, Quigley HA, Dunkelberger GR. Retinal ganglion cell loss is size dependent in experimental glaucoma. *Invest Ophthalmol Vis Sci*. 1991;32:484–491.
4. Desatnik H, Quigley HA, Glovinsky Y. Study of central retinal ganglion cell loss in experimental glaucoma in monkey eyes. *J Glaucoma*. 1996;5:46–53.
5. Garcia-Valenzuela E, Shareef S, Walsh J, Sharma SC. Programmed cell death of retinal ganglion cells during experimental glaucoma. *Exp Eye Res*. 1995;61:33–44.
6. Nickells RW. Apoptosis of retinal ganglion cells in glaucoma: an update of the molecular pathways involved in cell death. *Surv Ophthalmol*. 1999;43(suppl 1):S151–S161.
7. Morgan JE, Uchida H, Caprioli J. Retinal ganglion cell death in experimental glaucoma. *Br J Ophthalmol*. 2000;84:303–310.
8. Morgan JE. Retinal ganglion cell shrinkage in glaucoma. *J Glaucoma*. 2002;11:365–370.
9. Pavlidis M, Stupp T, Naskar R, Cengiz C, Thanos S. Retinal ganglion cells resistant to advanced glaucoma: a postmortem study of human retinas with the carbocyanine dye DiI. *Invest Ophthalmol Vis Sci*. 2003;44:5196–5205.
10. Guo L, Moss SE, Alexander RA, Ali RR, Fitzke FW, Cordeiro MF. Retinal ganglion cell apoptosis in glaucoma is related to intraocular pressure and IOP-induced effects on extracellular matrix. *Invest Ophthalmol Vis Sci*. 2005;46:175–182.
11. Reichstein D, Ren L, Filippopoulos T, Mittag T, Danias J. Apoptotic retinal ganglion cell death in the DBA/2 mouse model of glaucoma. *Exp Eye Res*. 2007;84:13–21.
12. Holcombe DJ, Lengefeld N, Gole GA, Barnett NL. Selective inner retinal dysfunction precedes ganglion cell loss in a mouse glaucoma model. *Br J Ophthalmol*. 2008;92:683–688.
13. Fu QL, Li X, Shi J, et al. Synaptic degeneration of retinal ganglion cells in a rat ocular hypertension glaucoma model. *Cell Mol Neurobiol*. 2009;29:575–581.
14. Urcola JH, Hernandez M, Vecino E. Three experimental glaucoma models in rats: comparison of the effects of intraocular pressure elevation on retinal ganglion cell size and death. *Exp Eye Res*. 2006;83:429–437.
15. Wax MB, Tezel G. Immunoregulation of retinal ganglion cell fate in glaucoma. *Exp Eye Res*. 2009;88:825–830.
16. Quigley HA, Nickells RW, Kerrigan LA, Pease ME, Thibault DJ, Zack DJ. Retinal ganglion cell death in experimental glaucoma and after axotomy occurs by apoptosis. *Invest Ophthalmol Vis Sci*. 1995;36:774–786.
17. Saleh M, Nagaraju M, Porciatti V. Longitudinal evaluation of retinal ganglion cell function and IOP in the DBA/2J mouse model of glaucoma. *Invest Ophthalmol Vis Sci*. 2007;48:4564–4572.
18. Soto I, Oglesby E, Buckingham BP, et al. Retinal ganglion cells downregulate gene expression and lose their axons within the optic nerve head in a mouse glaucoma model. *J Neurosci*. 2008;28:548–561.
19. Perry VH, Oehler R, Cowey A. Retinal ganglion cells that project to the dorsal lateral geniculate nucleus in the macaque monkey. *Neuroscience*. 1984;12:1101–1123.
20. Yücel YH, Zhang Q, Gupta N, Kaufman PL, Weinreb RN. Loss of neurons in magnocellular and parvocellular layers of the lateral geniculate nucleus in glaucoma. *Arch Ophthalmol*. 2000;118:378–384.
21. Weber AJ, Chen H, Hubbard WC, Kaufman PL. Experimental glaucoma and cell size, density, and number in the primate lateral geniculate nucleus. *Invest Ophthalmol Vis Sci*. 2000;41:1370–1379.
22. Yücel YH, Zhang Q, Weinreb RN, Kaufman PL, Gupta N. Atrophy of relay neurons in magno- and parvocellular layers in the lateral geniculate nucleus in experimental glaucoma. *Invest Ophthalmol Vis Sci*. 2001;42:3216–3222.
23. Yücel YH, Zhang Q, Weinreb RN, Kaufman PL, Gupta N. Effects of retinal ganglion cell loss on magno-, parvo-, koniocellular pathways in the lateral geniculate nucleus and visual cortex in glaucoma. *Prog Retin Eye Res*. 2003;22:465–481.
24. Chaturvedi N, Hedley-Whyte ET, Dreyer EB. Lateral geniculate nucleus in glaucoma. *Am J Ophthalmol*. 1993;116:182–188.
25. Gupta N, Ang LC, Noël de Tilly L, Bidaisee L, Yücel YH. Human glaucoma and neuronal degeneration in intracranial optic nerve, lateral geniculate nucleus, and visual cortex. *Br J Ophthalmol*. 2006;90:674–678.
26. Horton JC, Landau K, Maeder P, Hoyt WF. Magnetic resonance imaging of the human lateral geniculate body. *Arch Neurol*. 1990;47:1201–1206.
27. Fujita N, Tanaka H, Takanashi M, et al. Lateral geniculate nucleus: anatomic and functional identification by use of MR imaging. *Am J Neuroradiol*. 2001;22:1719–1726.
28. Kleinschmidt A, Merboldt KD, Haenicke W, Steinmetz H, Frahm J. Correlational imaging of thalamocortical coupling in the primary visual pathway of the human brain. *J Cereb Blood Flow Metab*. 1994;14:952–957.
29. Chen W, Kato T, Zhu XH, Strupp J, Ogawa S, Ugurbil K. Mapping of lateral geniculate nucleus activation during visual stimulation in human brain using fMRI. *Magn Reson Med*. 1998;39:89–96.
30. Buechel C, Turner R, Friston K. Lateral geniculate activations can be detected using intersubject averaging and fMRI. *Magn Reson Med*. 1997;38:691–694.
31. Chen W, Zhu XH, Thulborn KR, Ugurbil K. Retinotopic mapping of lateral geniculate nucleus in humans using functional magnetic resonance imaging. *Proc Natl Acad Sci U S A*. 1999;96:2430–2434.
32. Logothetis NK, Guggenberger H, Peled S, Pauls J. Functional imaging of the monkey brain. *Nat Neurosci*. 1999;2:555–562.
33. Miki A, Liu GT, Raz J, et al. Visual activation in functional magnetic resonance imaging at very high field (4 Tesla). *J Neuroophthalmol*. 2001;21:8–11.
34. Gupta N, Greenberg G, de Tilly LN, Gray B, Polemidiotis M, Yücel YH. Atrophy of the lateral geniculate nucleus in human glaucoma detected by magnetic resonance imaging. *Br J Ophthalmol*. 2009;93:56–60.
35. Dai H, Mu KT, Qi JP, et al. Assessment of lateral geniculate nucleus atrophy with 3T MR imaging and correlation with clinical stage of glaucoma. *Am J Neuroradiol*. 2011;32:1347–1353.

36. Zikou AK, Kitsos G, Tzarouchi LC, Astrakas L, Alexiou GA, Arqyropoulou MI. Voxel-based morphometry and diffusion tensor imaging of the optic pathway in primary open-angle glaucoma: a preliminary study. *Am J Neuroradiol*. 2012;33: 128–134.
37. Hernowo AT, Boucard CC, Jansonius NM, Hooymans JM, Cornelissen FW. Automated morphometry of the visual pathway in primary open-angle glaucoma. *Invest Ophthalmol Vis Sci*. 2011;52:2758–2766.
38. Zhang YQ, Li J, Xu L, et al. Anterior visual pathway assessment by magnetic resonance imaging in normal-tension glaucoma. *Acta Ophthalmol*. 2012;90:e295–e302.
39. Chen Z, Wang J, Lin F, Dai H, Mu K, Zhang H. Correlation between lateral geniculate nucleus atrophy and damage to the optic disc in glaucoma. *J Neuroradiol*. 2013;40:281–287.
40. Anderson DR, Patella VM. *Automated Static Perimetry*. 2nd ed. St. Louis: Mosby; 1999:152–153.
41. Mwanza JC, Oakley JD, Budenz DL, et al. Macular ganglion cell-inner plexiform layer: automated detection and thickness reproducibility with spectral domain-optical coherence tomography in glaucoma. *Invest Ophthalmol Vis Sci*. 2011;52: 8323–8329.
42. Mwanza JC, Durbin MK, Budenz DL, et al. Glaucoma diagnostic accuracy of ganglion cell-inner plexiform layer thickness: comparison with nerve fiber layer and optic nerve head. *Ophthalmology*. 2012;119:1151–1158.
43. Curcio CA, Allen KA. Topography of ganglion cells in human retina. *J Comp Neurol*. 1990;300:5–25.
44. Tamraz J. Neuroradiologic investigation of the visual system using magnetic resonance imaging. *J Clin Neurophysiol*. 1994; 11:500–518.
45. Korsholm K, Madsen KH, Frederiksen JL, Skimminge A, Lund TE. Recovery from optic neuritis: an ROI-based analysis of LGN and visual cortical areas. *Brain*. 2007;130:1244–1253.
46. Benjamini Y, Hochberg Y. Controlling the false discovery rate: a practical and powerful approach to multiple testing. *J R Stat Soc Series B Stat Methodol*. 1995;57:289–300.
47. Malepli JG, Baker FH. The representation of the visual field in the lateral geniculate nucleus of macaca mulatta. *J Comp Neurol*. 1975;161:569–594.
48. Connolly M, Van Essen D. The representation of the visual field in parvicellular and magnocellular layers of the lateral geniculate nucleus in the macaque monkey. *J Comp Neurol*. 1984;226:544–564.
49. Kupfer C. The projection of the macula in the lateral geniculate nucleus of man. *Am J Ophthalmol*. 1962;54:597–609.
50. Hickey TL, Guillery RW. Variability of laminar patterns in the human lateral geniculate nucleus. *J Comp Neurol*. 1979;183: 221–246.
51. Schneider KA, Richter MC, Kastner S. Retinotopic organization and functional subdivisions of the human lateral geniculate nucleus: a high-resolution functional magnetic resonance imaging study. *J Neurosci*. 2004;24:8975–8985.
52. Putnam TJ. Studies on the central visual system. IV. The details of the organization of the geniculostriate system in man. *Arch Neurol*. 1926;16:683–707.
53. Zvorykin VP. New data on individual quantitative features of the human lateral geniculate body [in Russian]. *Arkh Anat Gistol Embriol*. 1980;78:24–27.
54. Andrews TJ, Halpern SD, Purves D. Correlated size variations in human visual cortex, lateral geniculate nucleus and optic tract. *J Neurosci*. 1997;17:2859–2868.
55. Li M, He HG, Shi W, et al. Quantification of the human lateral geniculate nucleus in vivo using MR imaging based on morphometry: volume loss with age. *Am J Neuroradiol*. 2012;33:915–921.
56. Kastner S, Schneider KA, Wunderlich K. Beyond a relay nucleus: neuroimaging views on the human LGN. *Prog Brain Res*. 2006;155:125–143.

Investigative Ophthalmology & Visual Science